Frustrated Frustration of Arrays with Four-Terminal Nb-Pt-Nb Josephson Junctions

Justus Teller, ^{1,2,*} Christian Schäfer, ^{1,2} Kristof Moors, ^{1,2,†} Benjamin Bennemann, ³ Matvey Lyatti, ^{1,2} Florian Lentz, ⁴ Detlev Grützmacher, ^{1,2} Roman-Pascal Riwar, ⁵ and Thomas Schäpers, ^{1,2,‡} ¹ Peter Grünberg Institut (PGI-9), Forschungszentrum Jülich, 52425 Jülich, Germany, ² JARA-Fundamentals of Future Information Technology, Jülich-Aachen Research Alliance, Forschungszentrum Jülich and RWTH Aachen University, 52425 Jülich, Germany, ³ Peter Grünberg Institut (PGI-10), Forschungszentrum Jülich, 52425 Jülich, Germany, ⁴ Helmholtz Nano Facility, Forschungszentrum Jülich, 52425 Jülich, Germany, ⁵ Peter Grünberg Institut (PGI-2), Forschungszentrum Jülich, 52425 Jülich, Germany

(Received 24 June 2025; accepted 16 September 2025; published 9 October 2025)

We study the frustration pattern of a square lattice with *in situ* fabricated Nb-Pt-Nb four-terminal Josephson junctions. The four-terminal geometry gives rise to a checkerboard pattern of alternating fluxes f, f' piercing the plaquettes, which stabilizes the Berezinskii-Kosterlitz-Thouless transition even at irrational flux quanta per plaquette, due to an unequal repartition of integer flux sum f + f' into alternating plaquettes. This type of frustrated frustration manifests as a beating pattern of the dc resistance, with state configurations at the resistance dips gradually changing between the conventional zero- and half-flux states. Hence, the four-terminal Josephson junction array offers a promising platform to study previously unexplored flux and vortex configurations and provides an estimate on the spatial expansion of the four-terminal Josephson junction central weak link area.

DOI: 10.1103/gxdc-py56

Introduction—Arrays of Josephson junctions have been studied since the 1980s [1] and a broad base of knowledge about the physics of these arrays has been accumulated over the years [2–19]. Recent findings in the field include the engineering of energy-phase relations with arrays [20], a deeper understanding of the vortex-lattice states in arrays [21], the demonstration of giant fractional Shapiro steps in anisotropic arrays [22], and the creation of arrays made of superconducting islands on a normal-conducting weak link material [22–26].

Typically, Josephson junction arrays are formed by twoterminal junctions. Recently, however, multiterminal Josephson junctions received increasing attention [27–31]. In general, a multiterminal Josephson junction is defined by multiple superconducting leads being connected by a central weak link region [28,31]. Various weak link materials can be used for these multiterminal Josephson junctions. There is a broad spectrum of studies of devices with weak links such as semiconductors [32–36], graphene [29,37–39], and

Published by the American Physical Society under the terms of the Creative Commons Attribution 4.0 International license. Further distribution of this work must maintain attribution to the author(s) and the published article's title, journal citation, and DOI. topological insulators [40–43]. Topological-insulator-based multiterminal Josephson junctions are considered as a key element in various Majorana fermion braiding architectures [44–46]. More generally, a multiterminal Josephson junction is predicted to host topological states without requiring any topological material [28].

We here report on the fabrication and study of a square array comprising multiterminal Josephson junctions, as illustrated in Fig. 1(a). In contrast to conventional Josephson junction arrays, where a two-terminal Josephson junction (2TJJ) is placed in each arm, forming a plaquette of the array, here, a four-terminal Josephson junction (4TJJ) is located in each corner of the unit cell. As it turns out, this system has not a single flux parameter (as usual arrays do) but an alternating pattern of two fluxes. This allows us to find a stable superconducting phase for the array, even for irrational fluxes piercing the individual plaquettes. Our Letter thus connects vortex dynamics and the Berezinskii-Kosterlitz-Thouless (BKT) transition to the emerging field of incommensurable, quasiperiodic physics in solid-state systems [47–52]. While the usual notion of quasiperiodic materials refers to lattices in real space, the incommensurability here is detectable in the space spanned by the applied flux.

Experiments—Our 4TJJ array is based on a superconductor–normal conductor structure, using a metal as a weak link between the superconducting electrodes [1,6,22,25,27,53]. More specifically, we use Nb for the four closely spaced superconducting electrodes connected by a metallic Pt weak link. The Nb electrodes induce

^{*}Contact author: j.teller@fz-juelich.de

[†]Present Address: Imec, Kapeldreef 75, 3001 Leuven, Belgium.

[‡]Contact author: th.schaepers@fz-juelich.de

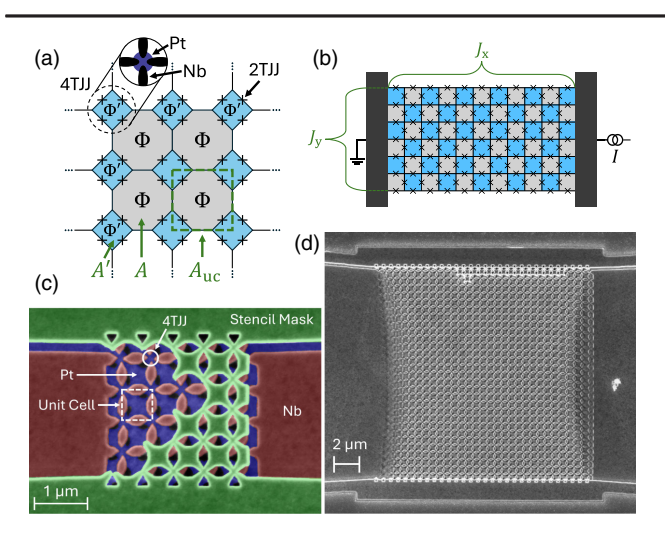


FIG. 1. (a) Schematics of the Josephson junction array where each 4TJJ is described by four interconnected two-terminal Josephson junctions (see dashed circle) [29,30,37,39]. Their weak link material is platinum (see inset). The array is formed by connecting the superconducting arms of the 4TJJs. Upon application of a magnetic field, each large plaquette area (A) of the array is penetrated by a magnetic flux Φ and the 4TJJ weak link area (A') by a flux Φ' . (b) Theoretical representation of the array shown in (a) as a 2TJJ array with square plaquettes having alternating frustrations $f = \Phi/\Phi_0$ (gray) and $f' = \Phi'/\Phi_0$ (blue). (c) False-color scanning electron micrograph of a 5×5 fourterminal Josephson junction array with partially removed stencil mask. The Pt (blue) is deposited under rotation and, thus, covers a larger area. The Nb (red) forms the superconducting contacts. The dashed square represents unit cell area $A_{\rm uc}$. (d) Scanning electron micrograph of the 30×30 4TJJ array presented in this Letter. Because of the shadow evaporation process, the 4TJJ array is slightly deformed at the left and right ends of the array.

superconductivity in the Pt directly beneath them. In the resistive array state, the induced superconductivity is maintained, while only the Josephson junctions become resistive [54]. The manufacturing process of the 4TJJ array is based on a stencil lithography process using molecular beam epitaxy with a high device yield by ensuring ultraclean interfaces between the Nb and Pt layers [63] (see Fig. 1 and Supplemental Material [54]).

Figure 1(d) shows a scanning electron microscope image of the 30×30 4TJJ array investigated in this Letter. In addition to the device presented in the main text, we measured an identical array device and a reference two-terminal Josephson junction, all fabricated on the same substrate during the same fabrication run [54].

Magnetotransport measurements have been performed on a 30×30 4TJJ array at a temperature of 80 mK. Without external magnetic field, the array shows a critical current of $I_c = 57 \mu A$ and, close to the superconducting regime, the device has a differential resistance of around 5.5 Ω [54].

The differential resistance versus bias current and out-ofplane magnetic field depicted in Fig. 2(a) shows periodic

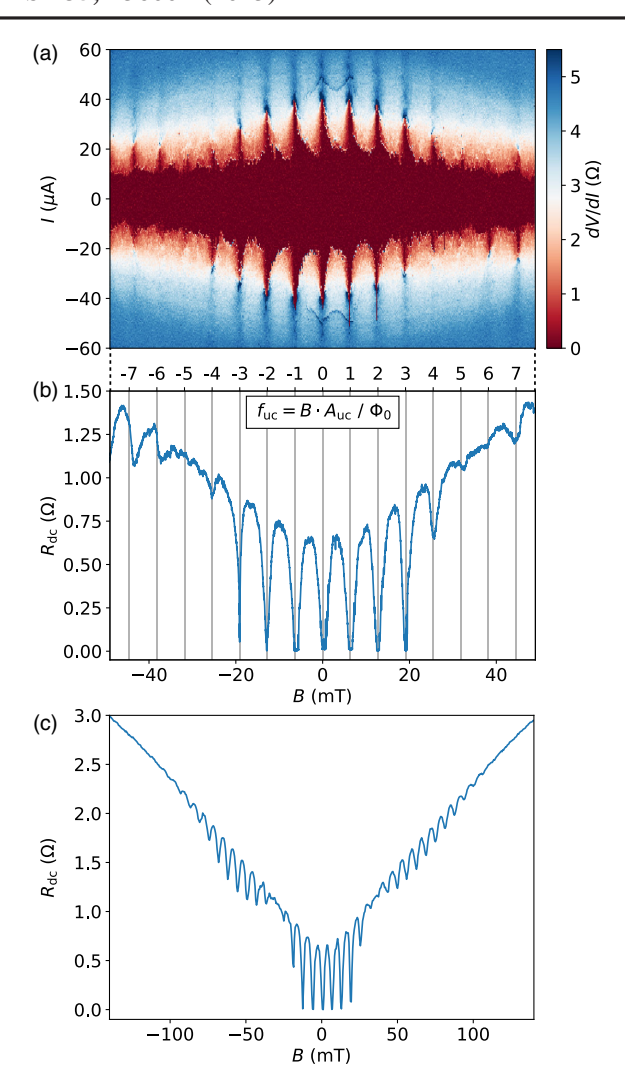


FIG. 2. Measurement data of the 30×30 4TJJ array at 80 mK. (a) Differential resistance as a function of bias current and magnetic field. A periodic oscillation of the critical current is clearly visible. (b) Resistance as a function of magnetic field with an applied dc bias of $30~\mu A$. The resistance oscillations correspond to a periodicity of 6.25~mT. At around $\pm 5f_{uc}$, the resistance oscillations are damped. (c) Resistance oscillations under magnetic field ranging to $\pm 140~mT$ with an applied dc bias of $30~\mu A$. In total, about 30~flux quantum oscillations are present.

oscillations of the critical current with magnetic field. When applying a fixed dc current of 30 μ A through the device, its resistance oscillates with the same periodicity in magnetic field [cf. Fig. 2(b)], which was determined to be 6.25 mT by a fast Fourier transform [54]. In addition, a device- and array-independent magnetic hysteresis of the resistance pattern was measured, also present in the reference 2TJJ and both arrays, which is not discussed further in the main text (see Sec. V in the Supplemental Material [54]).

To describe the properties of Josephson junction arrays, the so-called frustration parameter $f = BA/\Phi_0$, with A being the respective plaquette area, B the magnetic field

strength perpendicular to the array plane, and $\Phi_0 = h/2e$ the magnetic flux quantum, is used to characterize the magnetic resistance pattern, i.e., frustration pattern, see, e.g., Refs. [6,23]. It describes the average number of flux quanta piercing through an array plaquette. For rescaling the magnetic field into frustration, the unit cell area, as indicated in Fig. 1(c), has been determined to be $A_{\rm uc} = (570 \text{ nm})^2$ by scanning electron microscopy [54]. This unit cell is the sum of a large plaquette area A (with $\Phi = BA$) and a small plaquette area A' (with $\Phi' = BA'$) of Fig. 1(a), i.e., $A_{\rm uc} = A + A'$ (with $\Phi_{\rm uc} = BA_{\rm uc}$). The flux quantum oscillations of the resistance fit to $A_{\rm uc}$ in Fig. 2(b).

The resistance signal is similar to what, e.g., Rzchowski et al. [6] measured; however, the expected frustration pattern for rational values of f is missing. As can be seen in Figs. 2(b) and 2(c), at certain magnetic field around $\pm 5~f_{\rm uc}$, the oscillations first disappear and then reappear when further increasing the magnetic field. The resistance oscillations can be seen to magnetic fields above $\pm 100~{\rm mT}$ with, in total, about 30 flux quantum oscillations.

Theoretical discussion—To explain the measured behavior of the 4TJJ array, we introduce a corresponding theoretical model. Based on the resistively capacitively shunted junction (RCSJ) network model for multiterminal Josephson junctions [29,30,37,39], the array can be described, as shown in Fig. 1(a), with four 2TJJs creating one 4TJJ [54]. This introduces a second lattice of areas pierced by magnetic flux, the central weak link region of the 4TJJs. The multiterminal array model can, therefore, be conveniently represented in terms of an ordinary $J_x \times J_y$ square lattice junction model [where J_x and J_y are the horizontal and vertical number of superconducting nodes, see Fig. 1(b)], with the following important difference to previous theoretical and experimental studies: instead of all the plaquettes being pierced by the same flux, we get an alternating (checkerboard) flux pattern ($f = \Phi/\Phi_0$ and $f' = \Phi'/\Phi_0$). We deploy a classical RCSJ model approach, where the equations of motion for the superconducting phases at all nodes follow as usual from the Kirchhoff laws [54]. We focus on the overdamped regime [64], neglecting the capacitive contributions to the equations of motion, and assume zero temperature. As will become apparent below, it is instructive to include a Fraunhofer pattern [14] for the individual junctions in the lattice.

Including a source and drain contact on two sides of the lattice (across which the bias current I is applied), the RCSJ model allows for a direct computation of the dc resistance $R_{\rm dc}$ as a function of the magnetic field. We do so by an explicit numerical evaluation of the classical RCSJ equations of motion [65]. The results of the simulation are summarized in Fig. 3. For computational simplicity, the calculations were performed on a small array of $J_x = J_y = 6$. In the regime of interest, the results converge well already for such small lattices [54].

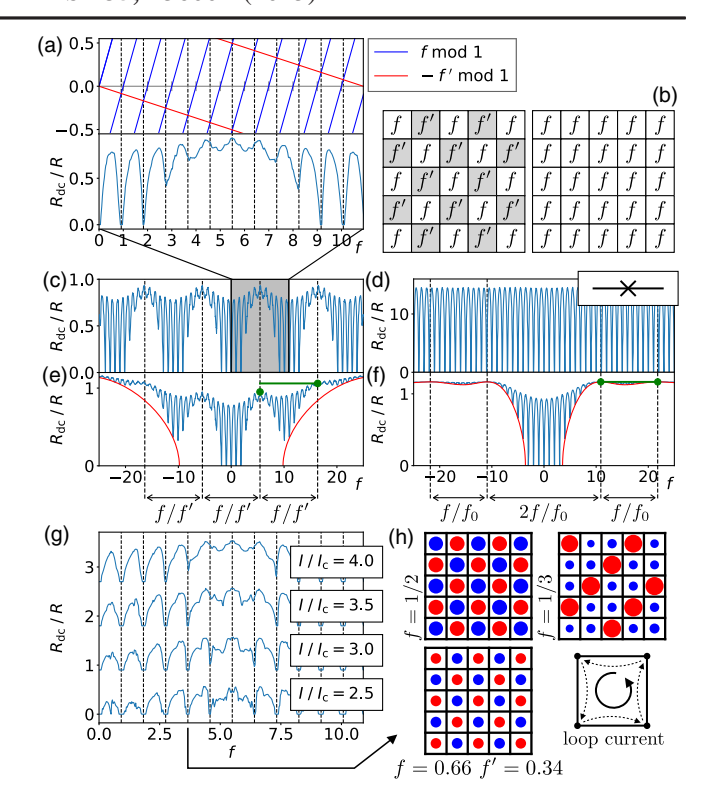


FIG. 3. Results of the theoretical analysis. In all curves (a),(c)–(g), the x axis is f, and the y axis is $R_{\rm dc}/R$. (a) $R_{\rm dc}$ as a function of f for the checkerboard model with f/f'=10.9 and $I/I_c=5.0$. (b) Checkerboard ($f \neq f'$) versus regular (f=f') lattice models. (c) Enlarged version of (a) showing the beating pattern. (d) $R_{\rm dc}$ for the regular lattice model f=f', with all other parameters the same as in (a),(c). (e),(f) $R_{\rm dc}$ including Fraunhofer pattern (red curves, see main text), where for the checkerboard model $f_0=30$ (e) and for the regular lattice $f_0=10.9$ (f). (g) $R_{\rm dc}$ for f/f'=10.9 (no Fraunhofer pattern) for decreasing bias current. Data shifted for clarification. (h) Equilibrium loop current configuration (I=0) for different values of f, f'. The dots indicate counter- (red) or clockwise (blue) going currents and their size represents the magnitude of the loop current (relative linear scale).

It is instructive to first consider the special case $f, f' \in \mathbb{Z}$ (equivalent to f = f' = 0). Here, the dc resistance can be found analytically (as both quantum and thermal phase slips are absent) [54],

$$\frac{R_{\rm dc}}{R} = (J_x + 1)\sqrt{\frac{1}{J_y^2} - \frac{I_c^2}{I^2}},\tag{1}$$

where R and I_c are the individual junction resistance and critical current, respectively. The array thus transitions from superconducting ($R_{\rm dc}=0$) to resistive ($R_{\rm dc}>0$) when the bias current exceeds J_yI_c . For a regular square lattice [f=f', see also Fig. 3(b)], it is well known that the array generally leaves the superconducting regime for noninteger values of f, even though $I < J_yI_c$. For sufficiently low temperatures and current biases, the dc resistance

nonetheless experiences dips at special rational values—known as the frustration pattern.

Consider now the general checkerboard array, $f \neq f'$ [left panel in Fig. 3(b)], where we denote the (constant) ratio $\beta = f/f' > 1$. Here, there emerges a beating pattern, with the two characteristic periods $\beta > 1$ and $\beta/(1+\beta) <$ 1 [see Figs. 3(a) and 3(c)]. The larger period (β) is, in general, only approximate; e.g., for incommensurate β the system can only approximately return to mutually integer f, f'—exhibiting a quasiperiodicity in flux space [66]. The irrational nature of β is, however, also highly relevant for the smaller period (which is exact): it separates the points where the sum of two neighboring plaquette fluxes is zero, i.e., $f + f' \in \mathbb{Z}$ [see top inset in Fig. 3(a)]. For the experimentally extracted value of $\beta \approx 10.9$ (cf. Fig. 2 and Supplemental Material [54]) the difference between the two frequencies is large, leading to a clearly visible beating pattern [Fig. 3(c)]. Once β is known, the central weak link area of a 4TJJ can be determined via $A' = A_{\rm uc}/$ $(1 + \beta)$, leading to $A' \approx (165 \text{ nm})^2$ [54]. Crucially, for integer f + f', the repartition of the total flux into the two neighboring plaquettes (f and f') does not need to occur for special (integer or rational) value, since the ratio of the two fluxes β is, in general, incommensurate. Consequently, the system exhibits a stabilization of the superconducting (BKT) phase (dips in R_{dc}) even for irrational f, f', a feature we choose to name "frustrated frustration."

We now include the Fraunhofer pattern, $I_c \sim \mathrm{sinc}(\pi f/f_0)$, where the parameter f_0 captures the junction area. The resulting reduction of the critical current at finite f leads to a base offset in the R_{dc} curve, see Fig. 3(e) [the red curve represents Eq. (1) with f-dependent I_c], in remarkable resemblance to the experimental data, Fig. 2(c). The good agreement of the patterns between theory and experiment indicates that current flow is relatively uniform through the junctions. Moreover, a magnetic-field-induced gap reduction can even further increase agreement between theory and experiment for large f. Taking the characteristic behavior of the gap for thin films [67], we get $I_c \sim \sqrt{1-\alpha f^2}$ (α depends on the critical field), providing an asymptotic behavior of R_{dc} linear in f.

In order to compare to an alternative possible model, take the regular square lattice, f=f', where a qualitatively very similar beating pattern arises due to the Fraunhofer pattern [Fig. 3(d) versus Fig. 3(f)], by setting f_0 (instead of f/f') to ≈ 10.9 . However, this alternative model can be safely excluded to explain the experimentally observed phenomenology. First, the Fraunhofer beating pattern in Fig. 3(f) skips a beat at f=0, due to the sinc function having no zero at the origin, such that there are two beating pattern frequencies, $2/f_0$ (main beat around f=0) and $1/f_0$ (side beats) [see Fig. 3(f)]. Figure 2 only exhibits one beating frequency, in alignment with the checkerboard model, Fig. 3(c). Moreover, the area ratio extracted from micrographs of the device align much better with the first model

 $(f/f' \approx 10.9)$ and much larger $\sim f_0$. Related to that, for $f/f_0 \ll 1$ (while $I \gg JI_c$), the base offset is approximately linear, $R_{\rm dc} \sim f$, consistent with the measured asymptotics in Fig. 2. Indeed, nodes separating two beats [green dots in Figs. 3(e) and 3(f)] can only exhibit an increase in $R_{\rm dc}$ in the checkerboard model, while in the regular lattice, the onset of the beating pattern must coincide with $R_{\rm dc}$ reaching the constant plateau value $\approx R$.

We observe that the pattern in Fig. 3(a) transitions from resistance dips to peaks at integer f + f', depending on whether f and f' are individually closer to integer or halfinteger. Those peaks can become dips when lowering the bias current, see Fig. 3(g), marking the onset of the checkerboard version of regular frustration—which goes hand in hand with the formation of additional resistance dips at f + f' half -integer [see, 0 < f < 1 in Fig. 3(g)] [68]. Overall, the frustrated frustration pattern $(f + f' \in \mathbb{Z})$ is more stable than regular frustration. For an intuitive understanding, consider the equilibrium (I = 0) configurations of loop currents [69] flowing through single plaquettes, see Fig. 3(h). Thus, we find that, e.g., the resistance dip at $f \approx 2/3$, $f' \approx 1/3$ resembles much more closely the configuration of f = f' = 1/2 than the one at f = f' = 1/3—however, with an overall reduced loop current magnitude, indicating increased stability. Stability considerations of the various frustration features can also be understood in terms of the regular vortex model [54]. Similarly, we notice that the f = 1/2 f' = 0 pattern studied in [70] can be realized thanks to frustrated frustration [54].

Conclusion—We demonstrated an array made with 4TJJs. For this we introduced an in situ fabrication technique for arrays. A frustration pattern was measured that differs from the expectation for ordinary 2TJJ arrays. The difference could be explained by theoretically introducing a checkerboard lattice with two alternating flux patterns f and f'. The periodicity of the beating pattern can be connected to the area ratios A/A'. In particular, while dips in the dc resistance can be linked to the sum f + f'being integer, the in general irrational area ratio leads to an irrational repartition of this total flux into the alternating plaquettes. This allows for the stabilization of the superconducting BKT phase at irrational fractions of flux penetrating individual plaquettes. This feature allows us to estimate the spatial expansion of the 4TJJ central weak link region, the result of which is compatible with the junction geometry. Overall, the here considered setup opens up a previously unexplored class of array system with alternating flux textures.

Outlook—Alternating f, f' lattice structures and their inherent flux incommensurability are expected to give rise to multifaceted follow-up research—also beyond superconducting circuits, due to the various well-known mappings from vortices to, e.g., spin lattices and solid-on-solid systems [71]. Specifically, half-flux configurations have been studied in the context of frustrated spin states ("triatic"

order) in the Kagome lattice [72–74] (which have so far escaped direct experimental confirmation in superconducting arrays) or in the form of π -shifted junctions (e.g., superconductor-ferromagnet-superconductor junctions [70] or d-wave junctions [75]), used to engineer nontrivial current-phase relationships with protected multiple minima [76,77]. We expect the concept of frustrated frustration to stabilize various such phenomena without the need for unconventional junction materials nor area fine-tuning. Finally, with the inclusion of vortex quantum fluctuations due to finite charging energies [8], it could be possible to observe different phase diagrams (due to the charge and dual flux offsets having fundamentally different statistics disordered versus ordered but incommensurate) or even to observe Anderson localizationlike features in charge or vortex space.

Acknowledgments—We thank Herbert Kertz for technical assistance and Ram Mummadavarapu for stimulating feedback. All samples have been prepared at the Helmholtz Nano Facility [78]. This work is funded by the Deutsche Forschungsgemeinschaft (DFG, German Foundation) under Germany's Excellence Strategy— Cluster of Excellence Matter and Light for Quantum Computing (ML4Q) EXC 2004/1-390534769, by the German Federal Ministry of Education and Research (BMBF) via the Quantum Future project "MajoranaChips" (Grant No. 13N15264), and the Quantum Future project with Grant No. 13N14891 (R.-P. R.), as well as the Bavarian Ministry of Economic Affairs, Regional Development and Energy within Bavaria's High-Tech Agenda Project "Bausteine für das Quantencomputing auf Basis topologischer Materialien mit experimentellen und theoretischen Ansätzen" (Grant No. 07 02/686 58/1/21 1/22 2/23).

Data availability—The data that support the findings of this article are openly available [79].

- [1] D. H. Sanchez and J.-L. Berchier, Properties of $n \times n$ square arrays of proximity effect bridges, J. Low Temp. Phys. **43**, 65 (1981).
- [2] D. W. Abraham, C. J. Lobb, M. Tinkham, and T. M. Klapwijk, Resistive transition in two-dimensional arrays of superconducting weak links, Phys. Rev. B 26, 5268 (1982).
- [3] C. J. Lobb, D. W. Abraham, and M. Tinkham, Theoretical interpretation of resistive transition data from arrays of superconducting weak links, Phys. Rev. B 27, 150 (1983).
- [4] S. Teitel and C. Jayaprakash, Josephson-junction arrays in transverse magnetic fields, Phys. Rev. Lett. **51**, 1999 (1983).
- [5] S. P. Benz, M. S. Rzchowski, M. Tinkham, and C. J. Lobb, Fractional giant Shapiro steps and spatially correlated phase motion in 2D Josephson arrays, Phys. Rev. Lett. 64, 693 (1990).

- [6] M. S. Rzchowski, S. P. Benz, M. Tinkham, and C. J. Lobb, Vortex pinning in Josephson-junction arrays, Phys. Rev. B 42, 2041 (1990).
- [7] J. E. Mooij, B. J. Van Wees, L. J. Geerligs, M. Peters, R. Fazio, and G. Schön, Unbinding of charge-anticharge pairs in two-dimensional arrays of small tunnel junctions, Phys. Rev. Lett. 65, 645 (1990).
- [8] R. Fazio and G. Schön, Charge and vortex dynamics in arrays of tunnel junctions, Phys. Rev. B 43, 5307 (1991).
- [9] U. Geigenmüller, C. J. Lobb, and C. B. Whan, Friction and inertia of a vortex in an underdamped Josephson array, Phys. Rev. B 47, 348 (1993).
- [10] E. K. F. Dang and B. L. Györffy, Vortex depinning in Josephson-junction arrays, Phys. Rev. B 47, 3290 (1993).
- [11] P. Martinoli and C. Leemann, Two dimensional Josephson junction arrays, J. Low Temp. Phys. **118**, 699 (2000).
- [12] R. Newrock, C. Lobb, U. Geigenmüller, and M. Octavio, The Two-dimensional physics of Josephson junction arrays, in *Solid State Physics* (Elsevier, New York, 2000), Vol. 54, pp. 263–512.
- [13] R. Fazio and H. van der Zant, Quantum phase transitions and vortex dynamics in superconducting networks, Phys. Rep. **355**, 235 (2001).
- [14] M. Tinkham, *Introduction to Superconductivity*, 2nd ed. (Dover Publications, New York, 2004).
- [15] C. Bruder, R. Fazio, and G. Schön, The Bose-Hubbard model: From Josephson junction arrays to optical lattices, Ann. Phys. (Berlin) **517**, 566 (2005).
- [16] A. Romito, R. Fazio, and C. Bruder, Solid-state quantum communication with Josephson arrays, Phys. Rev. B 71, 100501(R) (2005).
- [17] S. Gladchenko, D. Olaya, E. Dupont-Ferrier, B. Douçot, L. B. Ioffe, and M. E. Gershenson, Superconducting nanocircuits for topologically protected qubits, Nat. Phys. **5**, 48 (2009).
- [18] B. M. Terhal, F. Hassler, and D. P. DiVincenzo, From Majorana fermions to topological order, Phys. Rev. Lett. 108, 260504 (2012).
- [19] A. A. Houck, H. E. Türeci, and J. Koch, On-chip quantum simulation with superconducting circuits, Nat. Phys. **8**, 292 (2012).
- [20] A. M. Bozkurt, J. Brookman, V. Fatemi, and A. R. Akhmerov, Double-Fourier engineering of Josephson energy-phase relationships applied to diodes, SciPost Phys. 15, 204 (2023).
- [21] A.-G. Penner, K. Flensberg, L. I. Glazman, and F. von Oppen, Resistivity Tensor of vortex-lattice states in Josephson junction arrays, Phys. Rev. Lett. 131, 206001 (2023).
- [22] R. Panghotra, B. Raes, C. C. de Souza Silva, I. Cools, W. Keijers, J. E. Scheerder, V. V. Moshchalkov, and J. Van de Vondel, Giant fractional Shapiro steps in anisotropic Josephson junction arrays, Commun. Phys. 3, 53 (2020).
- [23] X. Song, S. Suresh Babu, Y. Bai, D. S. Golubev, I. Burkova, A. Romanov, E. Ilin, J. N. Eckstein, and A. Bezryadin, Interference, diffraction, and diode effects in superconducting array based on bismuth antimony telluride topological insulator, Commun. Phys. 6, 177 (2023).
- [24] C. G. L. Bøttcher, F. Nichele, J. Shabani, C. J. Palmstrøm, and C. M. Marcus, Dynamical vortex transitions in a

- gate-tunable two-dimensional Josephson junction array, Phys. Rev. B **108**, 134517 (2023).
- [25] S. Vervoort, L. Nulens, D. A. D. Chaves, H. Dausy, S. Reniers, M. Abouelela, I. P. C. Cools, A. V. Silhanek, M. J. V. Bael, B. Raes, and J. V. de Vondel, DC-operated Josephson junction arrays as a cryogenic on-chip microwave measurement platform, arXiv:2412.17576.
- [26] S. Reinhardt, A.-G. Penner, J. Berger, C. Baumgartner, S. Gronin, G. C. Gardner, T. Lindemann, M. J. Manfra, L. I. Glazman, F. von Oppen, N. Paradiso, and C. Strunk, Spontaneous supercurrents and vortex depinning in two-dimensional arrays of φ_0 -junctions, arXiv:2406.13819.
- [27] A. H. Pfeffer, J. E. Duvauchelle, H. Courtois, R. Mélin, D. Feinberg, and F. Lefloch, Subgap structure in the conductance of a three-terminal Josephson junction, Phys. Rev. B 90, 075401 (2014).
- [28] R.-P. Riwar, M. Houzet, J. S. Meyer, and Y. V. Nazarov, Multi-terminal Josephson junctions as topological matter, Nat. Commun. 7, 11167 (2016).
- [29] A. W. Draelos, M.-T. Wei, A. Seredinski, H. Li, Y. Mehta, K. Watanabe, T. Taniguchi, I. V. Borzenets, F. Amet, and G. Finkelstein, Supercurrent flow in multiterminal graphene Josephson junctions, Nano Lett. 19, 1039 (2019).
- [30] G. V. Graziano, J. S. Lee, M. Pendharkar, C. J. Palmstrøm, and V. S. Pribiag, Transport studies in a gate-tunable threeterminal Josephson junction, Phys. Rev. B 101, 054510 (2020).
- [31] N. Pankratova, H. Lee, R. Kuzmin, K. Wickramasinghe, W. Mayer, J. Yuan, M. G. Vavilov, J. Shabani, and V. E. Manucharyan, Multiterminal Josephson effect, Phys. Rev. X 10, 031051 (2020).
- [32] G. V. Graziano, M. Gupta, M. Pendharkar, J. T. Dong, C. P. Dempsey, C. Palmstrøm, and V. S. Pribiag, Selective control of conductance modes in multi-terminal Josephson junctions, Nat. Commun. 13, 5933 (2022).
- [33] M. Coraiola, D. Z. Haxell, D. Sabonis, H. Weisbrich, A. E. Svetogorov, M. Hinderling, S. C. ten Kate, E. Cheah, F. Krizek, R. Schott, W. Wegscheider, J. C. Cuevas, W. Belzig, and F. Nichele, Phase-engineering the Andreev band structure of a three-terminal Josephson junction, Nat. Commun. 14, 6784 (2023).
- [34] M. Gupta, G. V. Graziano, M. Pendharkar, J. T. Dong, C. P. Dempsey, C. Palmstrøm, and V. S. Pribiag, Gate-tunable superconducting diode effect in a three-terminal Josephson device, Nat. Commun. 14, 3078 (2023).
- [35] M. Coraiola, A. E. Svetogorov, D. Z. Haxell, D. Sabonis, M. Hinderling, S. C. Ten Kate, E. Cheah, F. Krizek, R. Schott, W. Wegscheider, J. C. Cuevas, W. Belzig, and F. Nichele, Flux-tunable Josephson diode effect in a hybrid four-terminal Josephson junction, ACS Nano 18, 9221 (2024).
- [36] M. Gupta, V. Khade, C. Riggert, L. Shani, G. Menning, P. Lueb, J. Jung, R. Mélin, E. P. A. M. Bakkers, and V. S. Pribiag, Evidence for π-shifted Cooper quartets and few-mode transport in PbTe nanowire three-terminal Josephson junctions, Nano Lett. 24, 13903 (2024).
- [37] E. G. Arnault, T. F. Q. Larson, A. Seredinski, L. Zhao, S. Idris, A. McConnell, K. Watanabe, T. Taniguchi, I. Borzenets, F. Amet, and G. Finkelstein, Multiterminal inverse AC Josephson effect, Nano Lett. 21, 9668 (2021).

- [38] J. Chiles, E. G. Arnault, C.-C. Chen, T. F. Q. Larson, L. Zhao, K. Watanabe, T. Taniguchi, F. Amet, and G. Finkelstein, Nonreciprocal supercurrents in a field-free graphene Josephson triode, Nano Lett. 23, 5257 (2023).
- [39] E. G. Arnault, S. Idris, A. McConnell, L. Zhao, T. F. Larson, K. Watanabe, T. Taniguchi, G. Finkelstein, and F. Amet, Dynamical stabilization of multiplet supercurrents in multiterminal Josephson junctions, Nano Lett. 22, 7073 (2022).
- [40] J. Kölzer, A. R. Jalil, D. Rosenbach, L. Arndt, G. Mussler, P. Schüffelgen, D. Grützmacher, H. Lüth, and T. Schäpers, Supercurrent in Bi₄Te₃ topological material-based three-terminal junctions, Nanomater. Nanotechnol. 13, 293 (2023).
- [41] G. Behner, A. R. Jalil, A. Rupp, H. Lüth, D. Grützmacher, and T. Schäpers, Superconductive coupling effects in selectively grown topological insulator-based three-terminal junctions, ACS Nano 19, 3878 (2025).
- [42] A. Kudriashov, X. Zhou, R. A. Hovhannisyan, A. Frolov, L. Elesin, Y. Wang, E. V. Zharkova, T. Taniguchi, K. Watanabe, L. A. Yashina, Z. Liu, X. Zhou, K. S. Novoselov, and D. A. Bandurin, Non-reciprocal current-phase relation and superconducting diode effect in topological-insulator-based Josephson junctions, arXiv:2502.08527.
- [43] E. Nikodem, J. Schluck, M. Geier, M. Papaj, H. F. Legg, J. Feng, M. Bagchi, L. Fu, and Y. Ando, Large tunable Josephson diode effect in a side-contacted topological-insulator-nanowire junction, arXiv:2412.16569.
- [44] L. Fu and C. L. Kane, Superconducting proximity effect and Majorana fermions at the surface of a topological insulator, Phys. Rev. Lett. **100**, 096407 (2008).
- [45] B. Van Heck, A. R. Akhmerov, F. Hassler, M. Burrello, and C. W. J. Beenakker, Coulomb-assisted braiding of Majorana fermions in a Josephson junction array, New J. Phys. 14, 035019 (2012).
- [46] I. C. Fulga, B. Van Heck, M. Burrello, and T. Hyart, Effects of disorder on Coulomb-assisted braiding of Majorana zero modes, Phys. Rev. B **88**, 155435 (2013).
- [47] S. J. Ahn, P. Moon, T.-H. Kim, H.-W. Kim, H.-C. Shin, E. H. Kim, H. W. Cha, S.-J. Kahng, P. Kim, M. Koshino, Y.-W. Son, C.-W. Yang, and J. R. Ahn, Dirac electrons in a dodecagonal graphene quasicrystal, Science 361, 782 (2018).
- [48] Y. Fu, E. J. König, J. H. Wilson, Y.-Z. Chou, and J. H. Pixley, Magic-angle semimetals, npj Quantum Mater. 5, 71 (2020).
- [49] E. Y. Andrei, D. K. Efetov, P. Jarillo-Herrero, A. H. MacDonald, K. F. Mak, T. Senthil, E. Tutuc, A. Yazdani, and A. F. Young, The marvels of moiré materials, Nat. Rev. Mater. 6, 201 (2021).
- [50] K. F. Mak and J. Shan, Semiconductor moiré materials, Nat. Nanotechnol. 17, 686 (2022).
- [51] A. Uri, S. C. de la Barrera, M. T. Randeria, D. Rodan-Legrain, T. Devakul, P. J. D. Crowley, N. Paul, K. Watanabe, T. Taniguchi, R. Lifshitz, L. Fu, R. C. Ashoori, and P. Jarillo-Herrero, Superconductivity and strong interactions in a tunable moiré quasicrystal, Nature (London) 620, 762 (2023).
- [52] T. Herrig, C. Koliofoti, J. H. Pixley, E. J. König, and R.-P. Riwar, Emulating moiré materials with quasiperiodic circuit

- quantum electrodynamics, Phys. Rev. B **111**, L201104 (2025).
- [53] O. V. Skryabina, S. V. Egorov, A. S. Goncharova, A. A. Klimenko, S. N. Kozlov, V. V. Ryazanov, S. V. Bakurskiy, M. Yu. Kupriyanov, A. A. Golubov, K. S. Napolskii, and V. S. Stolyarov, Josephson coupling across a long single-crystalline Cu nanowire, Appl. Phys. Lett. 110, 222605 (2017).
- [54] See Supplemental Material at http://link.aps.org/supplemental/10.1103/gxdc-py56 for fabrication procedure, measurement setup, additional measurement data, additional devices, additional data analysis, and additional theoretical discussion, as well as the estimation of β and the 4TJJ central weak link area, which includes Refs. [55–62].
- [55] H. Courtois, M. Meschke, J. T. Peltonen, and J. P. Pekola, Origin of hysteresis in a proximity Josephson junction, Phys. Rev. Lett. 101, 067002 (2008).
- [56] A. I. Gubin, K. S. Il'in, S. A. Vitusevich, M. Siegel, and N. Klein, Dependence of magnetic penetration depth on the thickness of superconducting Nb thin films, Phys. Rev. B 72, 064503 (2005).
- [57] K. Neurohr, Th. Schäpers, J. Malindretos, S. Lachenmann, A. I. Braginski, H. Lüth, M. Behet, G. Borghs, and A. A. Golubov, Local suppression of Josephson currents in niobium/two-dimensional electron gas/niobium structures by an injection current, Phys. Rev. B 59, 11197 (1999).
- [58] T. Schäpers, Superconductor/Semiconductor Junctions, edited by G. Höhler, J. Kühn, Th. Müller, A. Ruckenstein, F. Steiner, J. Trümper, P. Wölfle, and E. A. Niekisch, Springer Tracts in Modern Physics Vol. 174 (Springer, Berlin, Heidelberg, 2001).
- [59] M. Kockert, R. Mitdank, A. Zykov, S. Kowarik, and S. F. Fischer, Absolute seebeck coefficient of thin platinum films, J. Appl. Phys. 126, 105106 (2019).
- [60] D. P. Kennedy, Spreading resistance in cylindrical semiconductor devices, J. Appl. Phys. 31, 1490 (1960).
- [61] R. G. Mazur and D. H. Dickey, A spreading resistance technique for resistivity measurements on silicon, J. Electrochem. Soc. 113, 255 (1966).
- [62] M. W. Denhoff, An accurate calculation of spreading resistance, J. Phys. D 39, 1761 (2006).
- [63] P. Schüffelgen *et al.*, Selective area growth and stencil lithography for *in situ* fabricated quantum devices, Nat. Nanotechnol. **14**, 825 (2019).
- [64] Using the extracted values for individual junction capacitances, resistances, and critical currents, we estimate the Steward-McCumber parameter to be $\approx 5.4 \times 10^{-6}$, well within the overdamped regime.
- [65] We use the NDSolve routine on *Mathematica* for explicit evaluation of the equations of motion.

- [66] Note that the experimental fitting parameter f/f' = 10.9 is close to an integer (difference to next nearest integer is 11-10.9 = 0.1), such that in Fig. 3(c), this quasi periodicity is only visible after many periods ($\sim 1/0.1 = 10$), which is outside of the displayed range of the x axis.
- [67] D. H. Douglass, Magnetic field dependence of the superconducting energy gap, Phys. Rev. Lett. 6, 346 (1961).
- [68] Such extra features have not been detected in experiment, likely due to application of higher bias currents. Future experiments could be dedicated to the search of additional frustration features.
- [69] Our definition of loop currents, as shown in Fig. 3(h), is related to, but distinct from, the more commonly considered vortex picture.
- [70] S. M. Frolov, M. J. A. Stoutimore, T. A. Crane, D. J. Van Harlingen, V. A. Oboznov, V. V. Ryazanov, A. Ruosi, C. Granata, and M. Russo, Imaging spontaneous currents in superconducting arrays of π-junctions, Nat. Phys. 4, 32 (2008).
- [71] S. T. Chui and J. D. Weeks, Phase transition in the twodimensional coulomb gas, and the interfacial roughening transition, Phys. Rev. B 14, 4978 (1976).
- [72] A. B. Harris, C. Kallin, and A. J. Berlinsky, Possible Néel orderings of the Kagomé antiferromagnet, Phys. Rev. B 45, 2899 (1992).
- [73] K. Park and D. A. Huse, Superconducting phase with fractional vortices in the frustrated kagomé wire network at f = 1/2, Phys. Rev. B **64**, 134522 (2001).
- [74] O. Neyenhuys, M. V. Fistul, and I. M. Eremin, Long-range Ising spins models emerging from frustrated Josephson junctions arrays with topological constraints, Phys. Rev. B **108**, 165413 (2023).
- [75] D. A. Wollman, D. J. Van Harlingen, W. C. Lee, D. M. Ginsberg, and A. J. Leggett, Experimental determination of the superconducting pairing state in YBCO from the phase coherence of YBCO-Pb dc SQUIDs, Phys. Rev. Lett. **71**, 2134 (1993).
- [76] L. B. Ioffe, V. B. Geshkenbein, M. V. Feigel'man, A. L. Fauchère, and G. Blatter, Environmentally decoupled sds -wave Josephson junctions for quantum computing, Nature (London) **398**, 679 (1999).
- [77] M. T. Bell, J. Paramanandam, L. B. Ioffe, and M. E. Gershenson, Protected Josephson rhombus chains, Phys. Rev. Lett. 112, 167001 (2014).
- [78] W. Albrecht, J. Moers, and B. Hermanns, HNF—Helmholtz nano facility, J. Large-Scale Res. Facil. 3, A112 (2017).
- [79] J. Teller, C. Schäfer, K. Moors, B. Bennemann, M. Lyatti, F. Lentz, D. Grützmacher, R.-P. Riwar, and T. Schäpers, Data for: Frustrated Frustration of Arrays with Four-Terminal Nb-Pt-Nb Josephson Junctions, V1, Jülich DATA, 10.26165/JUELICH-DATA/O3EAHV, (2025).